Factors influencing residue cross section in ^{48}Ca-induced reactions

D. A. Mayorov, T. A. Werke, M. C. Alfonso, M. E. Bennett, and C. M. Folden III

In fusion reactions of ^{40}Ar with isotopes of lanthanide elements, Vermeulen et al. [1] observed surprisingly low production cross sections for weakly deformed elements near the N = 126 isotone line. In some cases, the measurement was up to a factor of 100 below predictions. The discrepancy was resolved by considering collective effects [2-4], which are most significant for production of weakly deformed nuclei. Rotational excitations enhance the nuclear level density at the fission saddle, while being absent for the near-spherical ground state of that nucleus. This in turn raises the fission probability for the excited nucleus formed in the fusion reaction in the ^{40}Ar experiments, while leaving the neutron emission channel unaffected. The same effects are of relevance to the field of transactinide elements ($Z \geq 103$), as present day efforts to produce ^{299}120 near the predicted shell closures Z = 120, N =184 are ongoing [5, 6]. However, there is a relatively small list of publications concerning this topic. Investigation on the production of weakly deformed nuclei in fusion reactions is, therefore, of particular interest. In the present report we show preliminary data for ^{48}Ca-induced reactions on targets of ^{154}Gd, ^{159}Tb, ^{162}Dy, and ^{165}Ho studied at the Cyclotron Institute. The products in these reactions are weakly deformed nuclides near the N = 126 shell. The measured difference in excitation functions can be understood in terms of a simple model for calculating survival probabilities dependent primarily on the fission barrier, B_f, and neutron separation energy, B_n. The ^{48}Ca data discussed here is part of a larger systematic study also including ^{50}Ti- and ^{54}Cr-induced reactions which is described in detail in [7].

Beams of $^{48}Ca^{6+}$ or $^{48}Ca^{7+}$ ($\approx$ 5 MeV/u) were delivered by the K500 cyclotron for irradiation of ^{154}Gd (1.0 mg/cm^2 $^{154}Gd_2O_3$ on 2 μm Ti), ^{159}Tb (497 μg/cm^2), ^{162}Dy (403 μg/cm^2 on 75 μg/cm^2 ^{nat}C), and ^{165}Ho (498 μg/cm^2) targets, in three temporally separated experiments. The ^{154}Gd target was prepared by molecular plating the metal nitrate salt on a 2 μm thick Ti backing foil, and is described in a separate contribution to this report. Beam dose on target was continuously monitored by two collimated ion-implanted Si charged-particle detectors positioned at ±30^{o} to the beam axis. The beam energy was varied using 0 (no degrader), 1.20, 2.25, 3.45, 4.50, 5.10, and 6.29 μm Al degraders in order to measure the excitation functions for the studied reactions. A ^{nat}C foil was also used for reaction residue charge equilibration. Products of interest would transverse the Momentum Achromat Recoil Spectrometer (MARS) [8] and implant into the focal plane position sensitive silicon detector. Discrimination between α-decays and implantation events was achieved by pulsing the beam or using an upstream micro-channel plate detector. The measured alpha spectra are shown in Fig. 1. In reactions with ^{162}Dy and ^{165}Ho targets, the 4n and 5n products have nearly identical half-lives and α-decay energies. Therefore, the alpha peak represents the sum of these two reaction products.

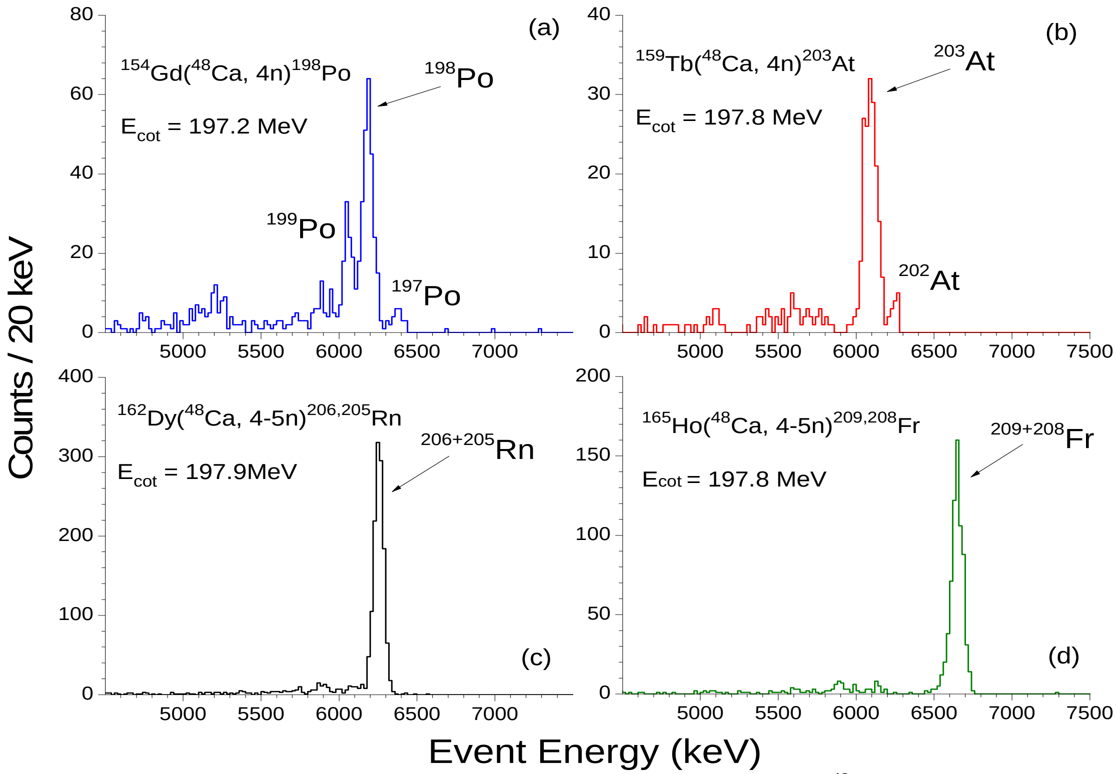

FIG. 1. Energy spectra for α-decaying evaporation residues produced in ^{48}Ca-induced reactions on lanthanides and implanted in a position-sensitive silicon detector placed at the focal plane of the MARS spectrometer.

Fig. 2a shows the measured excitation functions for the production of the 4*n* evaporation residues in reactions of ^{48}Ca with ^{154}Gd, ^{159}Tb, ^{162}Dy, and ^{165}Ho, plotted as a function of the laboratory-frame projectile energy at center-of-target, E_{cot}. Reactions with ^{159}Tb, ^{162}Dy, ^{165}Ho show a nearly invariable maximum cross section with the highest production cross section of 7.9±2.0 mb measured for the reaction ^{162}Dy(^{48}Ca, 4-5n)^{206,205}Rn. The maximum production cross section falls to 2.3±0.4 mb for the ^{154}Gd(^{48}Ca,4n)^{198}Po reaction.

The magnitude of B_f and B_n heavily influences the survival of the excited nucleus synthesized in the fusion reaction, and therefore the evaporation residue cross section. Fig. 2b shows the difference B_f - B_n plotted as a function of neutrons emitted in a series of neutron emission steps (up to 4*n*) from the excited compound system formed in each reaction. The fission barriers are calculated according to the refined rotating-liquid-drop-model [9] and neutron binding energies are taken from [10]. The use of highly neutron-rich ^{48}Ca results in relatively neutron-rich compound nucleus, thereby lowering the B_n of that nuclide relative to its lighter isotopes and aiding survival against fission. The clustering observed in Fig. 2b for all targets except ^{154}Gd suggests that the survival probability for these reactions should be equal in magnitude, which is consistent with the experimental data. In the case of the ^{154}Gd target, the smaller fission barriers and larger neutron separation energies reduce the production cross section.

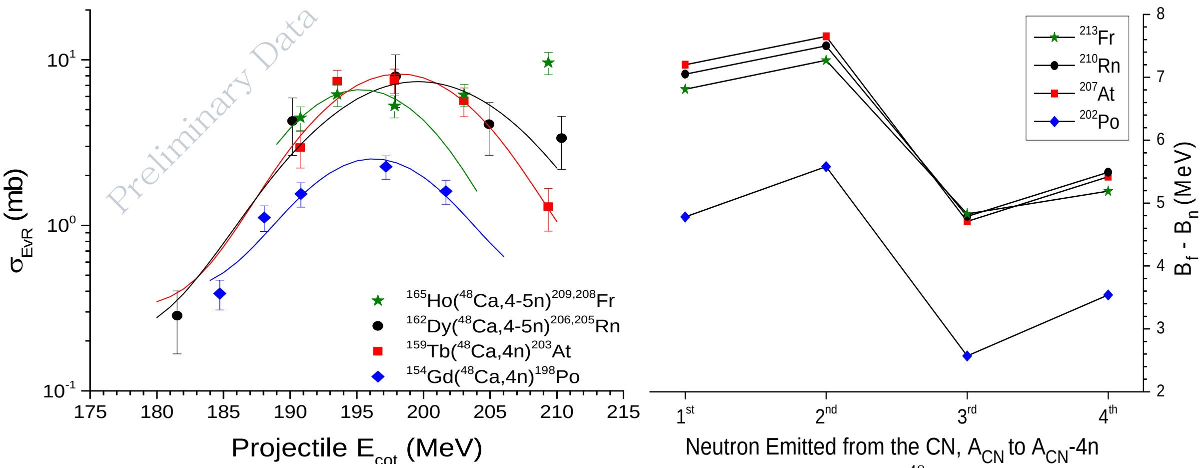

FIG. 2. *Left* (a): Excitation functions for the four-neutron emission channel for four ^{48}Ca-induced reactions. Note that the rise in the high-energy tail for the ^{48}Ca+^{165}Ho data is a transition from the 4n to the 5n product, both of which decay with nearly identical half-lives and alpha energies. Lines are drawn to guide the eye. *Right* (b): Plot of the difference in the fission barrier [9] and neutron separation energy [10] as a function of neutron emitted from the compound nucleus. The compound nucleus formed in each ^{48}Ca reaction is indicated in the legend.

The survival probability W_{sur} is expressed theoretically as [11]

$$W_{sur} = P\left(E^*_{CN}, x\right) \cdot \prod_{i=1}^{x} \left[\Gamma_n / \left(\Gamma_n + \Gamma_f\right)\right]_i \qquad (1)$$

where $P\left(E^*_{CN}, x\right)$ [12] determines the probability of emitting exactly x neutrons from an excited nucleus with excitation energy E^*_{CN}, Γ_n is the neutron decay width and Γ_f is the fission decay width. The decay width can be estimated from B_f and B_n using the method of Vandenbosch and Huizenga [13]:

$$\frac{\Gamma_n}{\Gamma_f} = \frac{4A^{2/3} a_f (E - B_n)}{K_o a_n [2a_f^{\;1/2}(E - B_f)^{1/2} - 1]} \exp[2a_n^{\;1/2}(E - B_n)^{1/2} - 2a_f^{\;1/2}(E - B_f)^{1/2}] \qquad (2)$$

with the level density having the form,

$$a_n = \tilde{a}_n [1 + (\delta S_n^{A-1} / E)(1 - \exp(-E/d))] \qquad (3)$$

$$a_f = \tilde{a}_f [1 + (\delta S_f^{A} / E)(1 - \exp(-E/d))] \qquad (4)$$

where E is the intrinsic excitation energy of the compound system, a is the energy-dependent level density parameter, $\tilde{a}$ is the energy-independent level density parameter, δS is the shell correction energy in the ground state for neutron emission or at the saddle point for fission, and $d \approx 16.4$ MeV [4]. Equation

2 models the "washing-out" of nuclear shell corrections [14]. The constant $K_o = \hbar^2 / g m_n r_o^2 \approx 9.8$ MeV, where g is the spin degeneracy and m_n the mass of the neutron, and r_o is the radius parameter.

Using Eq. 1-4 and including collective effects as prescribed in [4], W_{sur} for the 4n products of interest in each ^{48}Ca-induced reaction at E_{cot} corresponding to the maximum of each excitation function in Fig. 2a were calculated and are shown in column 7 of Table I. This simple model reproduces the ratios of the experimental cross sections to within a factor of ≈ 2. For instance, the ratio of experimental cross section $\sigma_{EvR}(^{206,205}\text{Rn}) / \sigma_{EvR}(^{198}\text{Po}) = 3.5 \pm 1.1$, while $W_{sur}(^{206,205}\text{Rn}) / W_{sur}(^{198}\text{Po}) \approx 1.8$. The ratio of the product of capture cross section and survival probability for these two reactions is ≈ 1.6.

The capture process describes the approach of the projectile to the target over an interaction barrier taken as the sum of Coulomb and nuclear forces. The diffused barrier formula [15] was used to calculate the capture cross section shown in Table I. In the above calculation, B_f at $l = 0$ were used with agreeable results. With increasing angular momentum, however, the liquid-drop fission barrier does diminish and entirely vanish at $l = l_{critical}$ [16]. This leads to a reduction in survival probability. Future analysis will incorporate the effect of average angular momentum on the production cross section. Furthermore, since experimental fission barrier data is not available for the neutron-deficient nuclides considered here, the impact of alternative models for fission barriers on W_{sur} should be examined. With W_{sur} having exponential dependence on B_f, a small change in the barrier height can produce a significant change in the survival probability.

Table I. Maximum measured 4n evaporation residue cross sections for ^{48}Ca+^{154}Gd, ^{159}Tb, ^{162}Dy, and ^{165}Ho reactions along with the corresponding projectile energies at center-of-target and excitation energy. Estimates of σ_{cap} and W_{sur} are given for the same energies.

E_{cot} (MeV)	E^*_{CN} (MeV)	Target	Residue	4n σ_{EvR} (mb)	σ_{cap} (mb)	W_{sur}
197.2	50.3	^{154}Gd	^{198}Po	2.3±0.4	180	0.30
197.8	51.4	^{159}Tb	^{203}At	7.5±1.3	185	0.63
197.9	49.9	^{162}Dy	^{206,205}Rn	7.9±2.0	163	0.54
197.8	47.7	^{165}Ho	^{209,208}Fr	5.3±0.8	138	0.42

The excitation functions for four ^{48}Ca-induced reactions on targets of ^{154}Gd, ^{159}Tb, ^{162}Dy, and ^{165}Ho have been measured. The measured production cross sections are highly correlated to $B_f - B_n$, which significantly affects the survival probability. Using a simple model for survival probability in preliminary analysis of the data, the differences observed in the maxima of the excitation functions can be explained, and it is the survival that plays a dominant role in the magnitude of the production cross section. Future work will continue excitation function measurements with ^{50}Ti and ^{54}Cr projectiles on the same targets to quantify the dependence of the cross section on the projectile.

[1] D. Vermeulen *et al.*, Z. Phys. A **318**, 157 (1984).
[2] P. Armbruster, Rep. Prog. Phys. **62**, 465 (1999).
[3] A.R. Junghans *et al.*, Nucl. Phys. **A629**, 635 (1998).

[4] V.I. Zagrebaev *et al.*, Phys. Rev. C **65**, 014607 (2001).
[5] M. Bender, and P.-H. Heenen, J. Phys.: Conf. Ser. **420**, 012002 (2013).
[6] Ch. E. Düllmann *et al.*, GSI Scientific Report (2011).
[7] C.M. Folden III *et al.*, J. Phys.: Conf. Ser. **420**, 012007 (2013).
[8] R.E. Tribble, R.H. Burch, and C.A. Gagliardi, Nucl. Instrum. Methods Phys. Res.**A285**, 441 (1989).
[9] A.J. Sierk, Phys. Rev. C **33**, 2039 (1986).
[10] *National Nuclear Data Center* (2013), available at http://www.nndc.bnl.gov.
[11] W. Loveland, J. Phys.: Conf. Ser. **420**, 012004 (2013).
[12] J.D. Jackson, Can. J. Phys. **34**, 767 (1956).
[13] R. Vandenbosch, and J.R. Huizenga, *Nuclear Fission* (Academic, New York, 1973), p.323.
[14] A.V. Ignatyuk, G.N. Smirenkin, and A.S. Tishin, Sov. J. Nucl. Phys, **21**, 255 (1975).
[15] W.J. Swiatecki, K. Siwek-Wilczynska, and J. Wilczynski, Phys. Rev. C **71**, 014602 (2005).
[16] S. Cohen, F. Plasil, and W. J. Swiatecki, Ann. Phys. **82**, 557 (1974).